*Published online 22 June 2017*

*Nucleic Acids Research, 2017, Vol. 45, No. 15* ***9093–9107***
*doi: 10.1093/nar/gkx536*

# ALG-5 is a miRNA-associated Argonaute required for proper developmental timing in the *Caenorhabditis elegans* germline

**Kristen C. Brown[1,2], Joshua M. Svendsen[1,2], Rachel M. Tucci[1], Brooke E. Montgomery[1] and Taiowa A. Montgomery[1,*]**

[1]Department of Biology, Colorado State University, Fort Collins, CO 80523, USA and [2]Cell and Molecular Biology Program, Colorado State University, Fort Collins, CO 80523, USA

Received May 14, 2017; Revised June 06, 2017; Editorial Decision June 09, 2017; Accepted June 09, 2017

## ABSTRACT

***Caenorhabditis elegans*** **contains 25 Argonautes, of which, ALG-1 and ALG-2 are known to primarily interact with miRNAs. ALG-5 belongs to the AGO subfamily of Argonautes that includes ALG-1 and ALG-2, but its role in small RNA pathways is unknown. We analyzed by high-throughput sequencing the small RNAs associated with ALG-5, ALG-1 and ALG-2, as well as changes in mRNA expression in *alg-5*, *alg-1* and *alg-2* mutants. We show that ALG-5 defines a distinct branch of the miRNA pathway affecting the expression of genes involved in immunity, defense, and development. In contrast to ALG-1 and ALG-2, which associate with most miRNAs and have general roles throughout development, ALG-5 interacts with only a small subset of miRNAs and is specifically expressed in the germline where it localizes alongside the piRNA and siRNA machinery at P granules. *alg-5* is required for optimal fertility and mutations in *alg-5* lead to a precocious transition from spermatogenesis to oogenesis. Our results provide a near-comprehensive analysis of miRNA-Argonaute interactions in *C. elegans* and reveal a new role for miRNAs in the germline.**

## INTRODUCTION

MicroRNAs (miRNAs) interact with target mRNAs to control the levels and timing of gene expression in plants and animals (1). miRNAs are processed from the stem regions of partially base-paired RNA hairpins into ∼22-nucleotide (nt) duplexes with 2-nt 3′ overhangs (2,3). miRNA duplexes form ribonucleoprotein complexes with effector proteins in the Argonaute/Piwi family, upon which, one of the two strands is ejected or degraded (4–6). The miRNA strand retained in the complex acts as a sequence-specific guide to anchor the Argonaute to a target mRNA, which in animals typically occurs via base-pairing between the seed region of the miRNA (nucleotides 2–8) and the 3′ UTR of the mRNA (7). miRNAs affect gene expression through two distinct modes—inhibition of translation or recruitment of mRNA decay factors. The individual contributions of these two modes of silencing can vary depending in part on the cellular context (8).

Small interfering RNAs (siRNAs) and piwi-interacting RNAs (piRNAs) are distinct classes of small RNAs related to miRNAs by their length (∼20–30-nt) and their association with Argonaute/Piwi proteins (9). The Argonautes can be classified into three subfamilies by their phylogenetic relatedness, which is often indicative of which of the three classes of small RNAs they bind. The AGO subfamily is conserved across eukaryotes and contains both miRNA and siRNA associated Argonautes, whereas Argonautes in the PIWI subfamily bind their namesake piRNAs. The WAGO subfamily is unique to nematodes and has thus far only been implicated in siRNA pathways. The nematode *Caenorhabditis elegans* contains each of the three broad classes of small RNAs, as well as 25 Argonautes spanning each of the three subfamilies (10). Each *C. elegans* Argonaute is specialized for a particular class or subclass of small RNAs, with the majority binding to the extensive repertoire of *C. elegans* siRNAs, which come in multiple varieties with distinct molecular features and functions (11).

The AGO subfamily of *C. elegans* Argonautes is comprised of five members, two of which, ALG-1 and ALG-2, interact with miRNAs, while two others, ALG-3 and ALG-4, function within the spermatogenesis branch of the 26-nt 5′G-containing siRNA (26G-RNA) pathway (11). RDE-1, which primarily associates with siRNAs and does not clearly fall within any of the Argonaute subfamilies, also binds a subset of miRNAs (12). HPO-24 (hereafter referred to as ALG-5 because of its relatedness to ALG-1–4), the fifth AGO subfamily Argonaute, has yet to be linked to a small RNA pathway.

*To whom correspondence should be addressed. Tel: +1 970 491 7198; Email: tai.montgomery@colostate.edu

We used protein-RNA co-immunoprecipitation combined with high-throughput sequencing to identify the small RNA interactors of ALG-5, as well as those of ALG-1 and ALG-2. We show that ALG-5 binds a subset of miRNAs that partially overlaps with those bound by ALG-1 and ALG-2. *alg-5* is expressed in the germline and ALG-5 protein localizes, in part, to P granules. Loss of *alg-5* activity results in a modest reduction in fertility and an accelerated transition from spermatogenesis to oogenesis in hermaphroditic animals. Using RNA-seq of *alg-5*, *alg-1* and *alg-2* mutants, we identified hundreds of mRNAs misregulated in the absence of each branch of the miRNA pathway. Of the mRNAs misregulated in *alg-5* mutants, genes involved in defense were most significantly enriched. The results implicate ALG-5 as a distinct germline-specific branch of the miRNA pathway and pave the way for functional analysis of the role of ALG-5 in immunity and development.

## MATERIALS AND METHODS

### Strains

N2 [wild type], VC446 [*alg-1(gk214)* X], WM53 [*alg-2(ok304)* II], WM159 [*alg-5(tm1163)* I], MT14119 [mir-35–41(nDf50)] and SS104 [*glp-4(bn2)* I] were obtained from the CGC. *RFP::pgl-1* was described in Gu *et al*. (13). The *alg-5(tm1163)* allele was backcrossed to wild type an additional two times. New strains generated for this study are listed in Supplementary Table S1. *alg-1::HA::alg-1, alg-2::HA::alg-2, alg-1::HA::alg-2, alg-5::HA::alg-5* and *alg-1::HA::alg-5* transgenes were generated using Life Technologies Multisite Gateway Technology. Individual promoter (∼2400–3700 nt upstream of start codon), CDS (start to stop codons), and 3′ UTR (∼400–1500 nt downstream of stop codon) sequences were PCR amplified from genomic DNA using Phusion polymerase (New England Biolabs). PCR products were cloned into entry vectors using Gateway BP recombination (Life Technologies). The HA epitope tag was PCR amplified from pENTR 3XHA-AGO1 (14) with primers that added a TEV tag and SpeI and NdeI restriction sites (Supplementary Table S2) and introduced into pENTR (Life Technologies). The 3XHA-TEV cassette was restriction digested from the pENTR plasmid using SpeI and NdeI and ligated into the *alg-1*, *alg-2* and *alg-5* CDS entry clones. Individual fragments were recombined into destination vectors modified for Life Technologies Multisite Gateway Technology (pCFJ151, *alg-5::HA::alg-5*, and pCFJ178, *alg-1::HA::alg-1, alg-2::HA::alg-2, alg-1::HA::alg-2*) (15). *alg-1::HA::alg-2* and *alg-1::HA::alg-5* were generated by recombining the *alg-1* promoter and 3′UTR sequences with the *alg-2* or *alg-5* CDS sequence, respectively. Constructs were sequence-verified and introduced into EG6699 [*ttTi5605* II; *unc-119(ed3)* III; oxEx1578] for integration on chromosome II (*alg-5::HA::alg-5, alg-1::HA::alg-5*) or EG5003 [*unc-119(ed3)* III; *cxTi10882* IV] for integration on chromosome IV (*alg-1::HA::alg-1, alg-2::HA::alg-2, alg-1::HA::alg-2*), using MosSCI (16). *alg-5(ram1[GFP::3xFLAG::alg-5 + loxP]), alg-5(ram2[GFP::3xFLAG + loxp])* and *alg-5(ram9[GFP::3xFLAG::alg-5$^{tm1163}$ + loxP]),* were generated using CRISPR/Cas9 as described in (17,18) using plasmids pDD162 and pDD282 (AddGene). Guide RNAs were designed using http://crispr.mit.edu/. Primer sequences are in Supplementary Table S2. Unless noted otherwise, strains were grown under standard conditions at 20°C (19).

### Phylogenetics

AGO clade Argonaute protein sequences (10) were aligned using ClustalW2 2.1 with the Dayhoff-PAM weight matrix (20). Protein maximum likelihood distances were calculated and the phylogenetic tree was drawn in Phylip 3.69 (21).

### Co-immunoprecipitation

Animals were grown at 20°C for 49 h (GFP::ALG-5) or 68 h (all HA::ALG strains) following L1 synchronization. Animals were flash frozen in liquid nitrogen and lysed in 50 mM Tris–Cl, pH 7.4, 100 mM KCl, 2.5 mM MgCl2, 0.1% Igepal CA-630, 0.5 mM PMSF and 1X Proteinase Inhibitor (Life Technologies, 88266). Cell debris was removed by centrifugation and cell lysates were incubated with anti-HA affinity matrix (Roche, 11815016001) or anti-GFP mAb-agarose (MBL, D153–8) for 1 h. Following co-immunoprecipitation (co-IP), beads were washed four times in lysis buffer and split into RNA and protein fractions.

### Protein isolation

Proteins were extracted from co-IPs or whole animals using Laemmli buffer. Embryos were extracted from gravid adults by hypochlorite treatment and incubated for ∼1 h in M9. L1 animals were collected after hatching and incubation for ∼24 h in M9. L2 animals were collected ∼20 h after L1 synchronization, L3 animals were collected ∼27 h after L1 synchronization. L4 animals were collected ∼48 h after L1 synchronization. Gravid adults were collected ∼68 h after L1 synchronization. For comparison of HA::ALG-5 levels in males and hermaphrodites, two replicates of 400 L4 stage animals of each sex were collected by hand picking animals ∼48 h after L1 synchronization of F1 animals from a self-cross between *alg-5::HA::alg-5* transgenic animals to enrich for males. For comparison of HA::ALG-5 and HA::ALG-1 levels in animals wild type for or deficient in germline proliferation, animals were treated with control (L4440) or *glp-4* dsRNA (22) and collected ∼68 h after L1 synchronization.

### Western blots

Proteins were resolved on 4–12% Bis–Tris SDS polyacrylamide gels and transferred to nitrocellulose membranes (Life Technologies). Blots were blocked in PBST containing 5% milk and probed with anti-HA (Roche, 12013819001), anti-actin (Abcam, ab3280) or anti-GFP antibodies (Invitrogen, MA5–15256-HRP). SuperSignal West Femto Maximum Sensitivity Chemiluminescent Substrate (Life Technologies, 34096) was used for signal detection. Where applicable, signal intensity was quantified on a Bio-Rad Chemi-Doc and HA-fusion protein levels were normalized to actin levels.

### RNA isolation

RNA was isolated from whole animals after flash freezing in liquid nitrogen or from input and co-IP fractions using Trizol (Life Technologies, 15596018) followed by two chloroform extractions and isopropanol precipitation. RNA was diluted to 1.0 ± 0.05 ug/ul prior to library preparation and qRT-PCR. For comparison of *alg-5*, *alg-1* and *alg-2* mRNA levels in wild type and *glp-4(bn2)* mutants, three biological replicate pools ($n = \sim$18,000 each) were collected as stage-matched young adults prior to the appearance of embryos in the uterus. For comparison of *alg-5* mRNA levels in males and hermaphrodites, three replicates of 50 L4 stage animals of each sex were collected by hand picking animals ∼48 h after L1 synchronization of F1 animals from a genetic cross between wild type animals to enrich for males.

### Small RNA sequencing

Small RNAs in the 18–28-nt range were purified from total RNA by size selection using electrophoretic transfer from 17% polyacrylamide gels. Purified small RNAs were treated with RNA polyphosphatase (Illumina, RP8092H) or Tobacco Alkaline Phosphatase (Epicentre Biotechnologies, T81050) to reduce di and triphosphates to monophosphates to facilitate capture of 22G-RNAs by 5′ adapter ligation. Phosphatase was deactivated and removed after 30 min by phenol:chloroform extraction. Preadenylated 3′ adapter was ligated to small RNAs using T4 RNA Ligase 2 Truncated KQ (NEB, M0373S). 5′ adapter was ligated using T4 RNA Ligase (Life Technologies, AM2140). Ligation reactions were done at 16°C for 16–18 h. Adapter-ligated small RNAs were size selected at each ligation step using electrophoretic transfer from 12 or 15% polyacrylamide gels. Adapter-bound small RNAs were reverse transcribed using SuperScript III (Life Technologies, 18080-044) and the Illumina TruSeq RT Primer. RT products were amplified using NEBNext 2X PCR Master Mix (NEB, M0541S) and the TruSeq forward primer and reverse primers containing index sequences. PCR products corresponding to 18–28-nt small RNAs (∼136–146 bp) were size selected using electrophoretic transfer from 10% polyacrylamide gels. Samples were sequenced on an Illumina HiSeq 2000, HiSeq 2500 or NextSeq 500. For each Argonaute analyzed, small RNA sequencing from co-IPs was done at least twice, and although results were consistent across experiments, for simplicity only one dataset is described. Primer and adapter sequences are in Supplementary Table S2.

### Small RNA sequencing data analysis

Small RNA sequences were parsed from adapters, filtered for quality, and aligned to the *C. elegans* genome (WS230) using CASHX 2.3 (23). The numbers of reads sequenced, parsed and mapped are described in Supplementary Table S3. Data analysis was done using R and custom Perl and Python scripts. miRNA annotation was based on miRBase release 20. Mutator class siRNA annotation was based on Phillips *et al.* (15). CSR-1 class siRNA annotation was based on Claycomb *et al.* (24). piRNA annotation was based on WormBase release WS230. New miRNAs were identified using miRDeep2 (25). To identify GFP::ALG-5, HA::ALG-5, HA::ALG-1 and HA::ALG-2 interactors, we calculated the normalized reads (reads per million total genome-matching reads in each library) in the small RNA libraries derived from the co-IP fractions relative to the cell lysate (input, in) fractions. HA::ALG-5 interactors were defined as miRNAs that were enriched in the co-IP fraction by >2-fold to account for presumed non-specific carryover from the cell lysates. Unless noted otherwise, a >1-fold cutoff was applied to HA::ALG-1, HA::ALG-2 and GFP::ALG-5 because these co-IPs had very little non-specific carryover from the cell lysates.

### mRNA sequencing

Methodology for mRNA library preparation was adapted from the NEBNext Ultra Directional RNA Library Prep Kit and Zhang *et al.* (26). RNA isolated from ∼5000 wild type, *alg-5(ram2)*, *alg-1(gk214)* and *alg-2(ok304)* mutant L4 stage animals per replicate (3 replicates per strain) was depleted of rRNA using the Ribo-Zero Magnetic Kit (Illumina, MRZH116). rRNA-depleted RNA was enriched for RNA >200 nucleotides using the RNA Clean & Concentrator-5 Kit (Zymo Research, R1015) and fragmented to 200–350 bp by incubating in SuperScript III 5X first strand buffer (Life Technologies) for 2 min at 94°C. First strand cDNA was synthesized from fragmented RNA using Superscript III RT and random hexamers (Life Technologies, 18080-093). Second strand cDNA was synthesized using the NEBNext Second Strand Synthesis Module (NEB, E7550S), which uses dUTP instead of dTTP to preserve strand information. Double-stranded cDNA was end repaired using NEBNext Ultra End Repair/dA-Tailing Module (NEB, E7442S). 200–350 bp double-stranded cDNA was size selected using AMPure XP Beads (Beckman Coulter, A63881). Adapters were ligated using T4 DNA Ligase (NEB, M0202S). Uracils were excised from cDNA using USER enzyme (NEB, M5505S) and cDNA strands that had contained uracil were degraded to prevent capture of the antisense strands. cDNA libraries were amplified by PCR. cDNA and PCR products were purified using AMPure XP Beads. Samples were sequenced on an Illumina HiSeq 2500. Primer and adapter sequences are in Supplementary Table S2.

### mRNA sequencing data analysis

Adapter sequences and low quality bases were trimmed from mRNA sequences using Trimmomatic 0.35 (27). Trimmed sequences were aligned to the *C. elegans* WS230 genome using TopHat2 (28). The numbers of reads sequenced, parsed, and aligned are described in Supplementary Table S3. Data processing and quality assessment were done using custom scripts in Python and R. Differentially regulated protein-coding genes were identified using Cuffdiff2 (29) and HTSeq-count followed by DESeq2 (30,31). rRNA, tRNA and mtRNA were masked from the analysis. A 1.5-fold-change cutoff was applied when filtering significantly affected genes. DAVID 6.8 was used to identify significantly overrepresented functional annotations using a Benjamini–Hochberg adjusted *P*-value cutoff of 0.05

(32,33). Categories were collapsed and colored the same in plots if there was >50% overlap of genes within the category containing fewer genes. Venn diagrams were generated using BioVenn (34). Reads were plotted in IGV 2.3.67 (35,36). Volcano plots were drawn with CummeRbund (29). miRNA target site abundance in differentially regulated genes was assessed using Targetscan Release 6.2 and custom scripts in Python and R (37,38).

### Quantitative RT-PCR

For qRT-PCR, Turbo DNase-treated total RNA (Life Technologies, AM1907) was subjected to reverse transcription with SuperScript III (Life Technologies, 18080-044) using an oligo(dT) primer to enrich for mRNA. qRT-PCR was done using iTaq Universal SYBR Green Supermix (Bio-Rad, 172-5122) and the primer sequences in Supplementary Table S2. Reverse transcription and qPCR were done according to manufacturers' specifications. qRT-PCR was done using a CFX96 Touch Real-Time PCR Detection System (Bio-Rad). Means and standard deviations were calculated for three biological replicates in each experiment. The $2^{-ddCT}$ method was used to quantify fold change differences between samples. *rpl-32* was used for normalization. P-values were calculated using ANOVA followed by either two-sample *t*-tests when making one comparison or Tukey HSD tests when making multiple comparisons.

### RNAi assays

Synchronized L1 animals were fed *E. coli* HT115 expressing either an empty vector control (L4440), or *alg-1*, *alg-2* or *glp-4* dsRNA (22).

### Phenotype assays

Animals were grown at 20°C on NGM plates containing live *E. coli* (OP50) unless noted otherwise. Brood size assays were done on individual animals over their entire lifetimes at 20°C or 25°C. Live progeny of each animal were counted and removed from the plates each day such that all hatched live animals were included in our counts. Dead embryos were not included. P-values for brood size assays were calculated using the Wilcoxon Rank Sum test. The numbers of animals that burst or had protruding vulvas were counted at 96–120 h. The timing of oogenesis was assayed in three independent experiments. Animals were scored as oogenic if the germline clearly contained at least one oocyte as evidenced by appearing as a larger, single-row, and often rectangular germ cell next to the spermatheca. Otherwise, if the gonad was clearly visible and did not appear to contain oocytes, the animal was scored as non-oogenic.

### Imaging

Imaging of live animals was done on a Zeiss Axio Imager Z2 upright microscope. Animals were immobilized in a 25 uM sodium azide solution on 1.5–2% Agarose pads. For assessing the presence or absence of oocytes, animals were imaged 56–61 h after L1 synchronization. For imaging GFP::ALG-5 and free GFP from *alg-5(ram2)*, the developmental stage was determined by the number of germ cells and the germline or whole animal morphology.

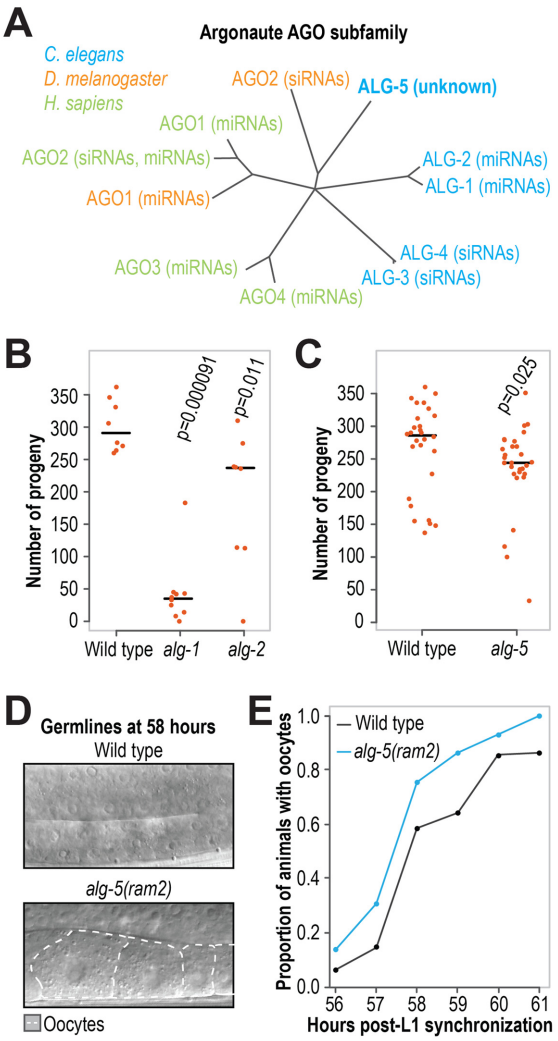


**Figure 1.** ALG-5 is required for optimal fertility and proper timing of oogenesis. (**A**) Phylogenetic tree of the AGO subfamily in worms, flies and humans. (**B**) Numbers of viable progeny produced by wild type ($n = 8$), *alg-1(gk214)* ($n = 10$) and *alg-2(ok304)* ($n = 8$) at 20°C. (**C**) Numbers of viable progeny produced by wild type ($n = 28$) and *alg-5(ram2)* ($n = 29$) grown at 20°C. (**D**) Representative images of wild type and *alg-5(ram2)* mutant germlines at 58 h post-L1 synchronization. The regions where oocytes form is shown. (**E**) Proportions of wild type and *alg-5(ram2)* mutant animals with oocytes formed at 56–61 h post-L1 synchronization ($n = \sim$25–50). One of three independent experiments is shown (the other two experiments are shown in Supplementary Figure S1D). At 58 h, the proportion of *alg-5(ram2)* mutant animals with oocytes is 17–35% higher than in wild type across the three experiments. See also Supplementary Figure S1.

## RESULTS

### ALG-5 is required for the proper developmental timing in the germline

ALG-5 is an AGO subfamily Argonaute most closely related in *C. elegans* to the miRNA-associated Argonautes ALG-1 and ALG-2 (~36% amino acid identity) (Figure 1A) (39). Whereas the role of ALG-5 is unknown, ALG-1 and ALG-2 have roles throughout development. *alg-1(gk214)* mutants display a strong reduction in the number of viable progeny they produce relative to wild type animals and *alg-*

*2(ok304)* mutants display a more modest reduction in viable progeny (Figure 1B) (39,40). The publically available partial deletion allele, *alg-5(tm1163)*, results in the loss of 145 amino acids in ALG-5, however, the mRNA is produced at near wild type levels outside of the deleted region (Supplementary Figure S1A). The protein produced by the *alg-5(tm1163)* allele is predicted to have a truncated PAZ domain, which engages the 3′ end of the small RNA, and to lack the linker 2 domain, which links the PAZ and PIWI lobes (Supplementary Figure S1B) (41). It is unclear, however, whether the mutation would result in complete loss of function phenotype. Thus, using CRISPR-Cas9 we developed an open reading frame deletion of *alg-5*, *alg-5(ram2)* in which the coding region was replaced with GFP sequence (Supplementary Figure S1B). Similar to what we observed in *alg-2(ok304)* mutants, *alg-5(tm1163)* mutants produced a median ∼24% fewer viable progeny than wild type animals ($P = 0.0015$, Supplementary Figure S1C) and *alg-5(ram2)* mutants produced ∼15% fewer progeny ($P = 0.025$, Figure 1C).

Aside from the modest reduction in brood size, neither *alg-5(tm1163)* nor *alg-5(ram2)* mutants displayed obvious developmental defects and in general appeared healthy, suggesting a specific requirement for ALG-5 in germline development or embryogenesis. Given the well-described heterochronic roles for small RNAs in *C. elegans*, we examined the timing of germ cell progression between spermatogenesis and oogenesis in wild type and *alg-5(ram2)* mutants. In each of three independent experiments, *alg-5(ram2)* mutants displayed precocious development of oocytes, pointing to an accelerated transition from spermatogenesis to oogenesis (Figure 1D and E and Supplementary Figure S1D). Our results therefore suggest that ALG-5 is required for the proper timing of oogenesis. The number of sperm produced in *C. elegans* hermaphrodites prior to oogenesis limits overall fecundity (42,43). Thus, the premature switch to oogenesis in *alg-5* mutants presumably reduces the number of sperm available for fertilization, likely resulting in the observed reduction in progeny.

### ALG-5 is primarily expressed in the germline

To determine when ALG-5 is expressed during development, we made an *HA::alg-5* epitope fusion transgene containing the endogenous *alg-5* 5′ and 3′ regulatory sequences and introduced it into *C. elegans* using Mos1-mediated single copy integration (16). We then crossed the transgene into the *alg-5(tm1163)* mutant strain and examined by western blot analysis HA::ALG-5 levels at each of the major developmental stages. Because of their relatedness to ALG-5, we also examined HA::ALG-1 and HA::ALG-2 levels across developmental stages using single-copy transgene strains developed for this study (see Materials and Methods). HA::ALG-5 expression was highest during late stages of larval development and into adulthood (Figure 2A and B). HA::ALG-1 was abundant throughout development, consistent with a central role for ALG-1 in the miRNA pathway (Figure 2C) (39,40,44–48). In contrast, HA::ALG-2 was predominantly expressed in embryos (Figure 2D).

The expression of HA::ALG-5 in late larval stages and adults (Figure 2B), the stages of development in which the *C. elegans* germline proliferates and matures, and the requirement of ALG-5 for the proper timing of oogenesis both point to a role for ALG-5 in germ cells. To determine if *alg-5* expression is elevated in germ cells relative to somatic cells, we measured by qRT-PCR *alg-5* mRNA levels in wild type and *glp-4(bn2)* mutant animals. When grown at the permissive temperature of 15°C, the germlines of *glp-4* mutants develop normally, but when grown at the non-permissive temperature of 25°C, the germlines fail to proliferate. Thus, a gene that is enriched in germ cells will be depleted in *glp-4* mutant animals grown at 25°C relative to animals grown at 15°C. *alg-5* levels were depleted ∼400-fold in *glp-4* mutants grown at 25°C relative to those grown at 15°C ($P = 2.1 \times 10^{-14}$) (Figure 2E). In contrast, *alg-1* mRNA levels were elevated >3-fold in *glp-4* mutants grown at 25°C relative to those grown at 15°C, indicating that *alg-1* is depleted in germ cells ($P = 0.00023$) (Figure 2E). *alg-2* mRNA levels were not significantly different between *glp-4* mutants grown at 15°C or 25°C ($P = 1.0$), suggesting that it is expressed in both somatic and germ cells (Figure 2E). Consistent with germline-specific expression, *alg-5* mRNA and protein levels were ∼2 fold higher in hermaphrodites, which contain two gonad arms, than in males, which contain a single gonad arm (Figure 2B).

To examine the tissue and cellular localization of ALG-5, we used CRISPR-Cas9 to introduce GFP sequence at the 5′ end of the coding sequence of the endogenous *alg*-5 locus in wild type animals (Supplementary Figure S1B) (17,18). Our *alg-5* deletion allele, *alg-5(ram2)*, described above also provides a transcriptional readout for *alg-5* expression, as it contains the *alg-5* 5′ and 3′ regulatory sequences flanking GFP coding sequence (Supplementary Figure S1B). Free GFP expressed from the *alg-5(ram2)* allele was present throughout development but was restricted to germ cells (Supplementary Figure S2A). Similarly, the GFP::ALG-5 fusion protein was detectable throughout development but only detectable above background in germ cells (Figure 2F). GFP::ALG-5 appeared cytoplasmically diffuse but also formed distinct puncta at the nuclear periphery reminiscent of P granules, a germ cell-specific class of RNA granules that function in mRNA surveillance. P granules contain the piRNA-associated Piwi protein, PRG-1, and much of the siRNA pathway machinery (49). GFP::ALG-5 foci overlapped with the P granule marker RFP::PGL-1 foci, indicating that, similar to many known piRNA and siRNA components, ALG-5 localizes to P granules (Figure 2F).

We also introduced GFP at the 5′ end of *alg-5* coding sequence in *alg-5(tm1163)* to determine if the mutant allele produces a stable protein (17,18). Indeed, GFP::ALG-$5^{tm1163}$ was expressed at similar levels to non-mutant GFP::ALG-5 protein and formed foci at the nuclear periphery (Supplementary Figure S2B). Because mutant ALG-5 produced from the *alg-5(tm1163)* allele could conceivably compete with other Argonautes for shared components of a small RNA pathway, it is important to interpret results obtained from the *alg-5(tm1163)* allele with caution.

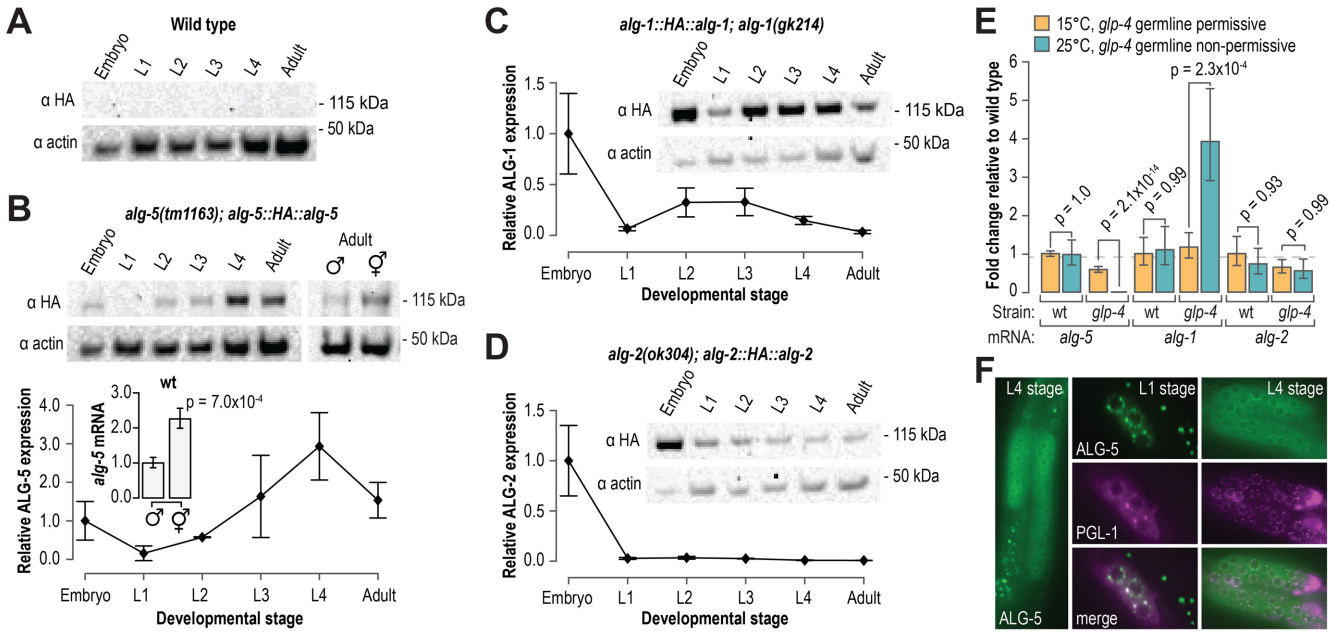


**Figure 2.** *alg-5* is specifically expressed in the germline. (**A**) Western blot assay of HA and actin in wild type animals across developmental stages. Non-transgenic wild type animals do not express the HA epitope and are included as a negative control. (**B**) Western blot assay and quantification of HA::ALG-5. A blot image of one of two biological replicates is shown. Points within the plot represent average signal intensity of HA normalized to actin (embryo sample arbitrarily set to 1.0). Error bars represent standard deviations from the mean. A western blot assay of HA::ALG-5 in hermaphrodites and males is also shown. The bar plot displays relative levels of endogenous *alg-5* mRNA in wild type animals, as determined by quantitative RT-PCR, in hermaphrodites and males. (**C** and **D**) Western blot assay and quantification of HA::ALG-1 (C) and HA::ALG-2 (D). Points within the plots represent average signal intensity of HA normalized to actin (embryo sample arbitrarily set to 1.0). Error bars represent standard deviations from the mean. (**E**) Average fold change in *alg-5, alg-1* and *alg-2* transcript levels in wild type and *glp-4(bn2)* at 15°C (orange) and 25°C (teal), as determined by quantitative RT-PCR. Error bars represent standard deviations from the means for three biological replicates. (**F**) Representative images of GFP::ALG-5 and RFP::PGL-1. Images are of GFP or RFP fluorescence in the germline regions of living animals. See also Supplementary Figure S2.

## ALG-5 functions in the miRNA pathway

To identify the small RNAs bound by ALG-5 and thus place ALG-5 within our current understanding of small RNA pathways, we co-immunoprecipitated GFP::ALG-5 and HA::ALG-5 protein complexes and subjected the associated small RNAs to high-throughput sequencing (Figure 3A and Supplementary Figure S3A). piRNAs, 22-nt 5′G-containing siRNAs (22G-RNAs), and 26G-RNAs were all depleted in both the GFP::ALG-5 and HA::ALG-5 co-immunoprecipitates (co-IPs), whereas miRNAs were enriched ∼2–3-fold (Figure 3B and C; Supplementary Figure S3A and B). Although as a class miRNAs were enriched, the majority of individual miRNAs were depleted in the ALG-5 co-IPs, as were individual piRNAs and 22G-RNA clusters (Figure 3D and Supplementary Table S4). Of the 368 annotated miRNAs in *C. elegans*, including both strands of each miRNA duplex, only 24 yielded >10 normalized reads (reads per million total mapped reads) and were enriched >1-fold in the GFP::ALG-5 co-IP. Of these, 10 were enriched >25-fold, indicating that ALG-5 binds with high affinity a very small number of miRNAs (Figure 3E). Although GFP::ALG-5 was co-immunoprecipitated from L4 stage animals and HA::ALG-5 from adult animals, there was nonetheless a majority overlap in the associated miRNAs (Figure 3E).

We next used small RNA high-throughput sequencing to assess miRNA accumulation defects in the two *alg-5* mutant strains, *alg-5(tm1163)* and *alg-5(ram2)*. Only one miRNA, miR-250-3p, was depleted >3-fold in the *alg-5(tm1163)* mutant (Supplementary Table S5). miR-250-3p was the fourth most highly enriched miRNA in the HA::ALG-5 co-IP (∼100-fold) and the fifth most highly enriched in the GFP::ALG-5 co-IP (∼140-fold), and its levels were partially rescued in *alg-5(tm1163)* by the *HA::alg-5* transgene (Supplementary Figure S3C and Table S4). Five miRNAs, including miR-250–3p, yielded >10 normalized reads and were depleted >3-fold in *alg-5(ram2)* mutants, only two of which were enriched in the GFP::ALG-5 co-IP (Figure 3F and Supplementary Table S5). Thus, the majority of miRNAs bound by ALG-5 are not dependent on ALG-5 for their overall stability, possibly because of association with other Argonautes, although they may be impacted specifically in the germline which might be missed in our whole animal-based approach.

## ALG-5, ALG-1 and ALG-2 interact with distinct subsets of miRNAs

To help determine the relatedness of ALG-5 to ALG-1 and ALG-2 within the miRNA pathway, we isolated small RNAs bound to HA-epitope fusions of ALG-1 and ALG-2 from adult animals and subjected them to high throughput sequencing (Supplementary Figure S4A). The majority of miRNAs were enriched in the HA::ALG-1 co-IP relative to the cell lysate (Figure 4A; Supplementary Figure S4B and

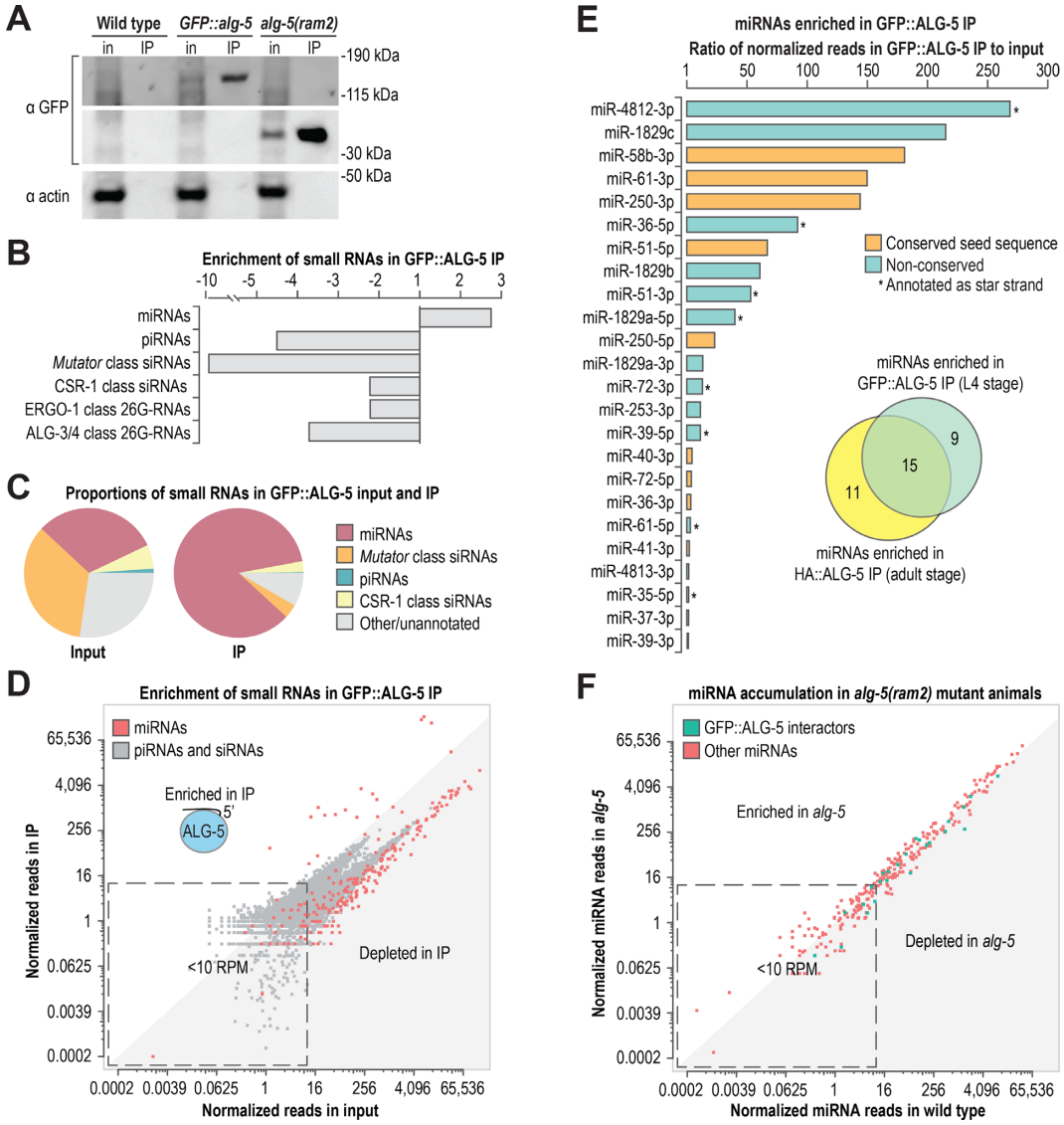


**Figure 3.** ALG-5 binds a subset of miRNAs. (**A**) Western blot assay of GFP::ALG-5 from cell lysates (input, in) and co-IPs (IP) used for small RNA isolation and sequencing. Wild type and *alg-5(ram2)* were included as controls. ∼0.2% starting material equivalents for the input fractions and ∼5% starting material equivalents for the co-IP fractions were run on the gels for western blots. (**B**) Enrichment of miRNAs, piRNAs, and siRNAs in GFP::ALG-5 co-IP relative to input as determined by high-throughput sequencing. (**C**) The relative proportions of each class of small RNAs in input and co-IP fractions. (**D**) Normalized reads (reads per million total mapped reads) for each miRNA in GFP::ALG-5 co-IP versus input are shown in red. Normalized reads for other classes of small RNAs (piRNAs and siRNA loci) are shown in gray. (**E**) miRNAs enriched >1-fold in the GFP::ALG-5 co-IP relative to input. Colors indicate if the seed sequence (positions 2–8) is conserved in *Drosophila melanogaster* and/or *Homo sapiens*. Asterisks indicate if the sequence is annotated as a star strand in miRBase v. 20. The inset Venn diagram displays the overlap in miRNAs enriched in the GFP::ALG-5 (L4 stage animals) and HA::ALG-5 (adult animals) co-IPs. (**F**) Normalized reads for each miRNA in *alg-5(ram2)* versus wild type. See also Supplementary Figure S3 and Tables S3–S5.

C; Supplementary Table S4). Most miRNAs were also depleted in *alg-1(gk214)* mutants, although this may be due in part to developmental defects in *alg-1* mutants (Figure 4B and Supplementary Table S5) (44,47). Total miRNA levels were depleted by ∼40% in *alg-1* mutants and were partially rescued by the *HA::alg-1* transgene (Supplementary Figure S4D).

Similar to HA::ALG-1, HA::ALG-2 interacted with the majority of miRNAs (Figure 4C; Supplementary Figure S4B and C; Table S4). However, unlike HA::ALG-1, which showed little bias for specific miRNAs, the HA::ALG-2 co-IP was strongly enriched for miR-35–42 family miRNAs, as well as miR-43, miR-51 and miR-1829a (∼10–24-fold) (Figure 4C and Supplementary Table S4). *alg-2(ok304)* mutants displayed only modest enrichment or depletion in the levels of most miRNAs, although members of the miR-35–42 family were depleted by ∼8–12-fold, except for miR-42 which was depleted by only ∼2-fold (Figure 4D; Supplementary Figure S4D; Supplementary Table S5). miR-35–42 levels in *alg-2(ok304)* mutants were partially restored by the *HA::alg-2* transgene (Supplementary Figure S4D). The miR-35 and miR-51 families are required for embryogenesis

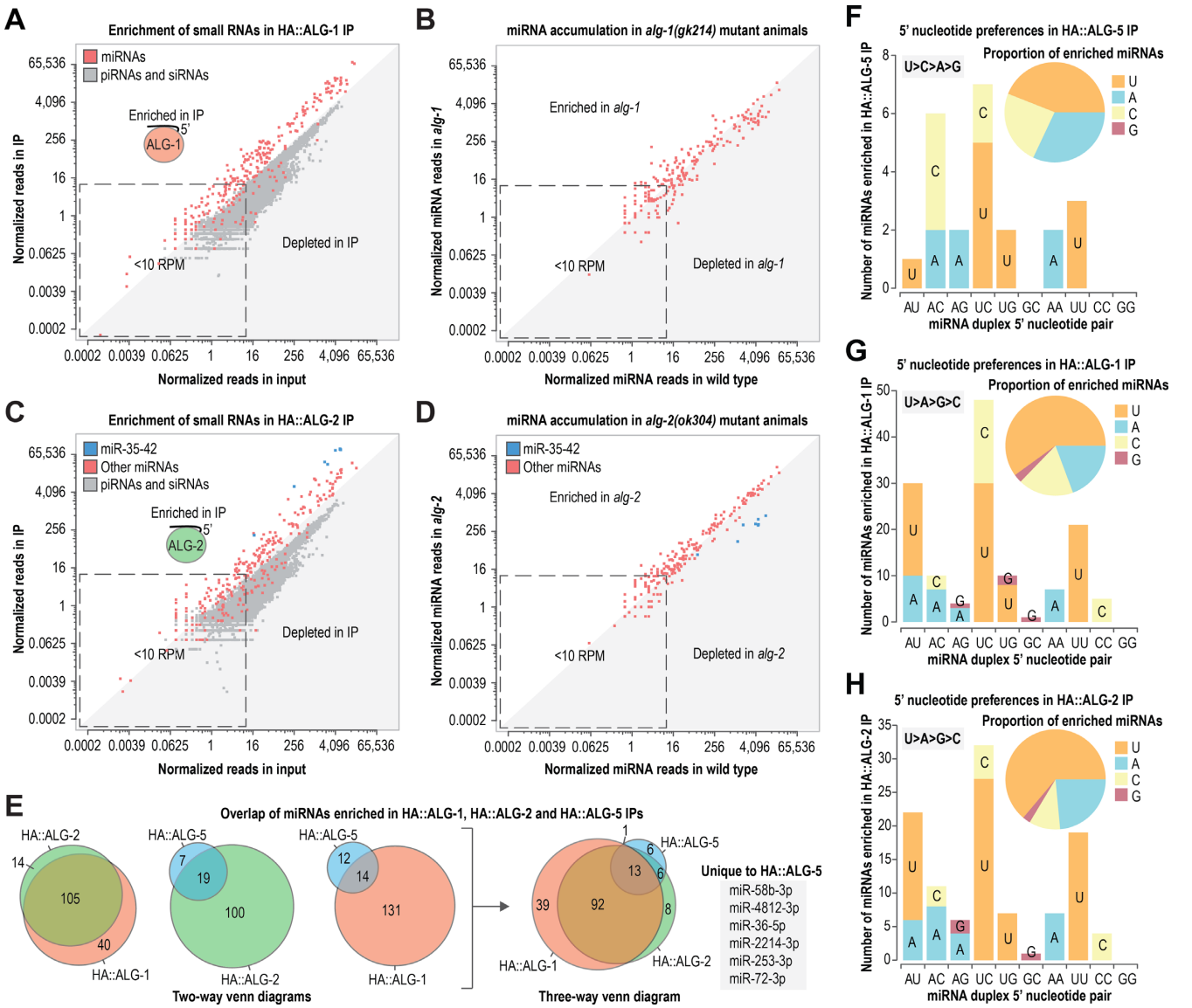


**Figure 4.** Overlap between miRNAs associated with ALG-5, ALG-1 and ALG-2. (**A**) Normalized reads for each miRNA in HA::ALG-1 co-IP versus input are shown in red. Normalized reads for other classes of small RNAs (piRNAs and siRNA loci) are shown in gray. (**B**) Normalized reads for each miRNA in *alg-1(gk214)* versus wild type. (**C**) Normalized reads for each miRNA in HA::ALG-2 co-IP versus input are shown in blue or red. Normalized reads for other classes of small RNAs (piRNAs and siRNA loci) are shown in gray. (**D**) Normalized reads for each miRNA in *alg-2(ok304)* versus wild type. (**E**) Overlap of miRNAs enriched in HA::ALG-1 and HA::ALG-2 co-IPs >1-fold and HA::ALG-5 IP >2-fold (data from adult stage animals). (**F-H**) Numbers of miRNAs enriched in HA::ALG-5 (F), HA::ALG-1 (G) and HA::ALG-2 (H) co-IPs categorized by 5′ nt. miRNAs are categorized by their 5′ nt and the 5′ nt of the opposing strand of the miRNA duplex. Only miRNA duplexes for which at least one strand was enriched in the corresponding co-IP are shown. Each bar corresponds to the total number of miRNA duplexes with each 5′ nt combination and each 5′ nt is shaded in a different color. See also Supplementary Figure S4 and Tables S3–S5.

(50). Thus, the strong enrichment we observed for miR-35 family miRNAs and miR-51 in the HA::ALG-2 co-IP and the relatively strong expression of HA::ALG-2 in embryos points to a prominent role for ALG-2 in conferring robustness to the miRNA pathway during embryogenesis (Figures 2D and 4C). In support of this model, we were unable to isolate animals homozygous mutant for both *alg-2* and *mir-35–41* (the *mir-35–41* deletion mutant has only a partially penetrant embryonic lethality phenotype because it contains wild type *mir-42*), suggesting that *alg-2* enhances the *mir-35–41* mutant phenotype (Supplementary Figure S4E) (50).

Of the 159 miRNAs that yielded >10 normalized reads (reads per million total mapped reads) and were enriched >1-fold in the HA::ALG-1 or HA::ALG-2 co-IPs, 14 were uniquely bound by HA::ALG-2 and 40 were uniquely bound by HA::ALG-1, based on this enrichment criterion (Figure 4E). Of the 26 miRNAs enriched in the HA::ALG-5 co-IP >2-fold (a 2-fold cutoff was used because of relatively high carryover from the cell lysate in the co-IP), 6 were depleted in both HA::ALG-1 and HA::ALG-2 co-IPs and were thus unique to HA::ALG-5, at least in adult animals (Figure 4E and Supplementary Table S4). We were

not able to identify unique sequence or structural features that might contribute to binding specificity among the Argonautes. Each of the three Argonautes preferentially bound miRNAs beginning with a uridine, although a greater proportion of miRNAs associated with HA::ALG-1 and HA::ALG-2 contained a 5′ uridine compared to HA::ALG-5 (Figure 4F–H).

Our small RNA high-throughput sequencing datasets from the co-IPs of GFP::ALG-5, HA::ALG-1 and HA::ALG-2 provided us with the opportunity to search for new miRNAs that might normally be missed due to their low abundance in whole animal cell lysates. Despite strong enrichment for miRNAs in these datasets, we identified only three new miRNAs, indicating that through the numerous high-throughput sequencing efforts, *C. elegans* miRNA identification is approaching saturation. miR-12001 is derived from a unique miRNA-generating locus and contains a novel seed sequence—positions 2–8, which are largely responsible for conferring miRNA-target recognition—placing it in a new miRNA family (Figure 5A) (7). The other two miRNAs are derived from genomic loci antisense (miR-12002) or adjacent (miR-12003) to annotated miRNA loci (Figure 5B and C). miR-12002 contains a novel seed sequence, thus defining a second new miRNA family (Figure 5B). miR-12003 shares a seed sequence with the miR-58/bantam family, and although not validated, was previously predicted to be a miRNA and shown to be downregulated in aged animals (Figure 5C) (51).

### Differential gene expression in *alg-5*, *alg-1* and *alg-2* mutants

To better understand the role of ALG-5 in regulating gene expression, we subjected total rRNA-depleted RNA from L4 stage wild type and *alg-5(ram2)* mutant animals to high-throughput mRNA sequencing. Differences in mRNA levels between wild type and mutant animals were quantified using Cuffdiff and HTSeq-count combined with DESeq (29–31) (Supplementary Tables S6 and S7). Applying a 1.5-fold change cutoff, we identified 88 upregulated and 235 downregulated genes in *alg-5(ram2)* using Cuffdiff (Figure 6A and Supplementary Tables S6 and S7). Because ALG-5 is expressed in the germline, in which several endogenous siRNA pathways function, we assessed whether the genes misregulated in *alg-5(ram2)* were targets of each of the germline siRNA pathways—Mutator, CSR-1, ALG-3/4 and ERGO-1. Among the downregulated genes, ∼26% are targets of siRNAs, representing a slight underrepresentation (1.6-fold) relative to what would be expected by chance, although Mutator targets were modestly enriched (∼1.3-fold) (Figure 6B). Within the upregulated gene set, only CSR-1 targets were enriched (∼1.2-fold) (Figure 6B). This was not unexpected given that ALG-5 functions in the germline and CSR-1 targets a large proportion of germline genes (24). We next assessed using DAVID overrepresentation of specific cellular processes within the gene sets differentially regulated in *alg-5* mutants (32,33). In the set of downregulated genes, several gene ontology terms related to immunity and defense were significantly enriched ($P < 0.05$) (Figure 6C and Supplementary Table S8). No specific gene ontology terms were significantly enriched by DAVID analysis within the upregulated gene set, likely due in part to its small size (88 genes from our Cuffdiff analysis).

In *C. elegans,* miRNAs guide gene silencing by affecting decay or translational repression of mRNA targets. However, the individual contribution of these two modes of silencing is poorly understood (8). It is possible that ALG-5 impacts gene expression through translational repression of its targets or that the genes that are misexpressed in *alg-5* mutants are downstream of the direct ALG-5 targets. Consistent with this possibility, we did not observe substantial enrichment for target sites (7-mers and 8-mers) of GFP::ALG-5-associated miRNAs within the mRNAs of genes up or downregulated in *alg-5* mutants (Supplementary Figure S5A). A similar lack of enrichment for targets sites was observed in miR-35 family mutants, in which genes that are misregulated are not enriched for miR-35 target sites (52). Nonetheless, the results suggest a role for ALG-5, be it direct or indirect, in regulating genes involved in development and defense response pathways.

In parallel to *alg-5(ram2)*, we assessed changes in gene expression in *alg-1(gk214)* and *alg-2(ok304)* mutant L4 stage animals. The *alg-1(gk214)* allele is a 220 bp deletion-13 bp insertion that deletes an exon–intron junction at the 5′ end of the coding sequence and would likely lead to a frame shift (Supplementary Figure S5B). The *alg-2(ok304)* allele is a 1378 bp deletion spanning much of the open reading frame (Supplementary Figure S5C). Both mRNAs are still expressed, although at much lower levels than from the wild type alleles (Supplementary Figure S5B and C). In *alg-1(gk214)*, 907 genes were upregulated >1.5-fold and 1163 genes were downregulated >1.5-fold as determined by Cuffdiff (Figure 6D and Supplementary Tables S9 and S10). In total, 2070 genes were misexpressed in *alg-1(gk214)*, representing nearly 10% of *C. elegans* protein coding genes. We were careful to stage match animals and removed developmentally delayed individuals from the pools of *alg-1(gk214)* mutants before collecting them for RNA isolation, however, it is possible that some of the genes misregulated in our dataset are artifacts of developmental abnormalities in *alg-1(gk214)*. In *alg-2(ok304)* mutants, which do not display obvious development abnormalities, we identified 1831 genes that were misregulated by >1.5-fold, of which 723 were upregulated and 1108 were downregulated using Cuffdiff (Figure 6E and Supplementary Tables S11 and S12). Numerous gene ontology terms were significantly enriched amongst the *alg-1(gk214)* and *alg-2(ok304)* misregulated gene sets, including defense response related terms (Figure 6F and G; Supplementary Tables S13–S16). However, the most highly enriched gene ontology terms identified amongst the *alg-1(gk214)* and *alg-2(ok304)* downregulated gene sets were related to phosphorus metabolism and protein phosphorylation and dephosphorylation (Figure 6F and G; Supplementary Tables S13 and S15). Classic targets of let-7 and lin-4, such as *lin-41* and *lin-14* respectively, were also among the genes significantly upregulated in *alg-1(gk214)* and *alg-2(ok304)* mutants (Supplementary Tables S10 and S12). Interestingly, and for reasons unclear to us, a large proportion of the genes downregulated in *alg-2(ok304)*, and to a lesser extent *alg-1(gk214)*, are also targets of the ALG-3/ALG-4 26G-RNA

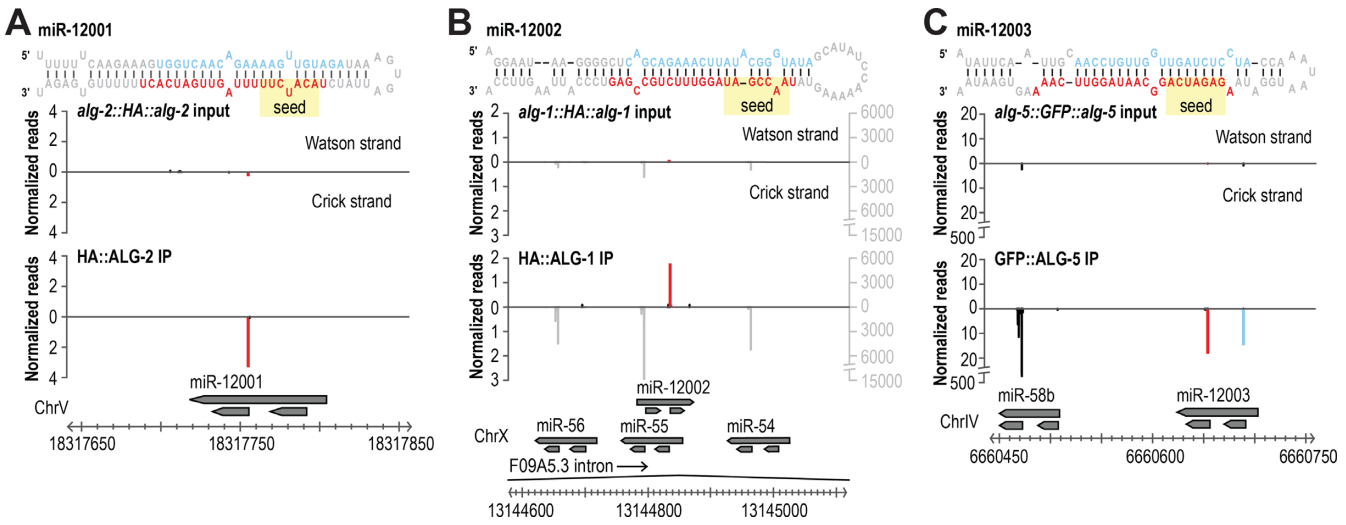


**Figure 5.** New miRNAs identified from Argonaute co-IPs. (**A**–**C**) miRNAs were identified by MirDeep2 using high-throughput sequencing data from GFP::ALG-5, HA::ALG-1 and HA::ALG-2 co-IPs. Small RNA distribution across each new miRNA locus in the co-IP library from which it was discovered and the corresponding input library. Names arbitrarily assigned and may differ in miRBase.

pathway that functions during sperm development (Figure 6B) (53–55).

There was substantial overlap in the genes misregulated in each of the miRNA-associated Argonaute mutants, particularly amongst the downregulated gene sets (Figure 6H). This is not unexpected given the overlap in miRNAs associated with each Argonaute (Figure 4E). However, given the differences we observed in expression of the Argonautes across developmental stages and their presence or absence in the germline (Figure 2), it is possible that there is tissue and timing specificity for each Argonaute even in regulating overlapping gene sets. We did not observe substantial enrichment for 7-mer and 8-mer target sites of miRNAs associated with HA::ALG-1 and HA::ALG-2 in the gene sets upregulated in the corresponding mutants (Supplementary Figure S5D and E). However, ∼75% of *C. elegans* genes are predicted to contain 7-mer or 8-mer target sites for miRNAs associated with HA::ALG-1 and HA::ALG-2 and thus there is very little room for enrichment (Supplementary Figure S5D and E) (37,38).

It is likely that many miRNA targets were missed in our analysis because of functional redundancy amongst the Argonautes and because our whole animal approach may dilute cell or tissue specific effects. It is also possible that many targets cannot be identified by RNA-seq because in some instances miRNAs may function in translational repression and not in mRNA decay, as noted above.

### Functional overlap between the miRNA-associated Argonautes

ALG-1 and ALG-2 have overlapping roles in development (39,44). To determine if ALG-5 has an overlapping role with ALG-1 or ALG-2, we introduced the *alg-5(ram2)* mutation into *alg-1(gk214)* and *alg-2(ok304)* mutant animals. *alg*-5 did not enhance the brood size defects of *alg-1* or *alg-2* mutants, nor did we observe additional developmental abnormalities not observed in the single mutants (Supplementary Figure S6A and B). It is nonetheless possible that there is redundancy between ALG-5 and the other Argonautes that would emerge from a more detailed analysis.

*alg-2*; *alg-1* double mutants arrest during embryogenesis (39,44). Suppressing *alg-2* by RNAi in *alg-1(gk214)* mutants during early larval stages also leads to developmental arrest, suggesting that ALG-1 and ALG-2 have overlapping roles during both embryo and larval development (Supplementary Figure S6C) (48). *alg-1* mutants are much sicker than *alg-2* mutants, thus it is possible that *alg-2* lacks certain functionality possessed by *alg-1*. To test this possibility, we developed a chimeric construct that contains the HA epitope sequence fused to the *alg-2* coding sequence and *alg-1* 5′ and 3′ regulatory sequences (*alg-1::HA::alg-2*) and introduced it into *alg-1(gk214)* mutant animals. HA::ALG-2 expressed under the control of *alg-1* regulatory elements displayed a similar expression profile to that of HA::ALG-1 (Figures 2C and 7A). Both the *alg-1::HA::alg-1* and *alg-1::HA::alg-2* transgenes rescued the developmental defects of *alg-1(gk214)* mutants, indicating ALG-2 is functionally interchangeable with ALG-1 (Figure 7B). The small RNA repertoire of HA::ALG-2 expressed from *alg-1* regulatory sequences had greater overlap with miRNAs uniquely bound by HA::ALG-1 than those uniquely bound by HA::ALG-2 (Figure 7C). This indicates that the difference we observed in miRNA specificity between HA::ALG-1 and HA::ALG-2 (Figure 4) does not reflect miRNA sequence or structure preferences of the two Argonautes and instead is likely due to developmental differences in *alg-1* and *alg-2* expression (Figure 2C and D).

Although we did not observe functional redundancy between *alg-5* and *alg-1*, we nonetheless tested whether ALG-5 is functionally interchangeable with ALG-1, as germline or somatic specificity in gene expression could preclude functional overlap during development. We developed a construct containing the HA epitope sequence fused to the *alg-5* coding sequencing and containing the *alg-1* 5′ and 3′ regulatory elements (*alg-1::HA::alg-5*) and introduced it by Mos1-mediated single copy integration into *C. ele-*

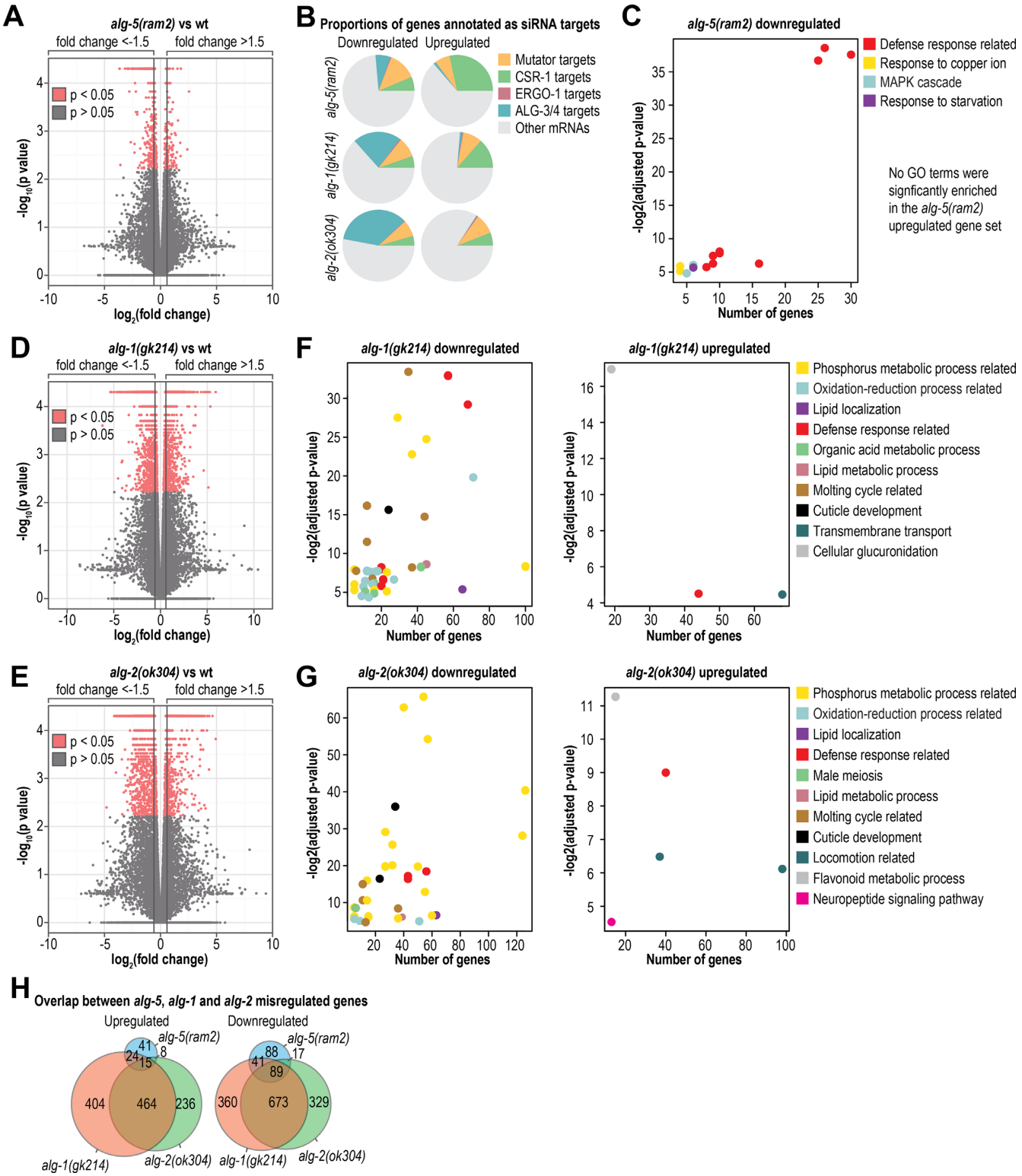


**Figure 6.** mRNA-seq analysis of differential gene expression in *alg-5*, *alg-1* and *alg-2* mutants. (**A**) Volcano plot displaying differential gene expression between *alg-5(ram2)* mutants and wild type animals ($n = 3$ replicate pools). (**B**) The proportions of genes misregulated in each of the Argonaute mutants that are also characterized as siRNA targets. (**C**) DAVID analysis of significantly enriched gene ontology terms amongst the genes misregulated in *alg-5(ram2)* mutants. Gene ontology categories are plotted as a function of the P value for enrichment and the number of genes associated with the gene ontology term. Some gene ontology terms overlap in associated genes by >50% and were collapsed into a more general category, as indicated in the key (e.g. 'Defense response related'). (**D**) Volcano plot displaying differential gene expression between *alg-1(gk214)* mutants and wild type animals ($n = 3$ replicate pools). (**E**) Volcano plot displaying differential gene expression between *alg-2(ok304)* mutants and wild type animals ($n = 3$ replicate pools). (**F**) Same as in C but *alg-1(gk214)*. (**G**) Same as in C but *alg-2(ok304)*. (**H**) Overlap in misregulated genes in each of the Argonaute mutants. See also Supplementary Figure S5 and Tables S6–S16.

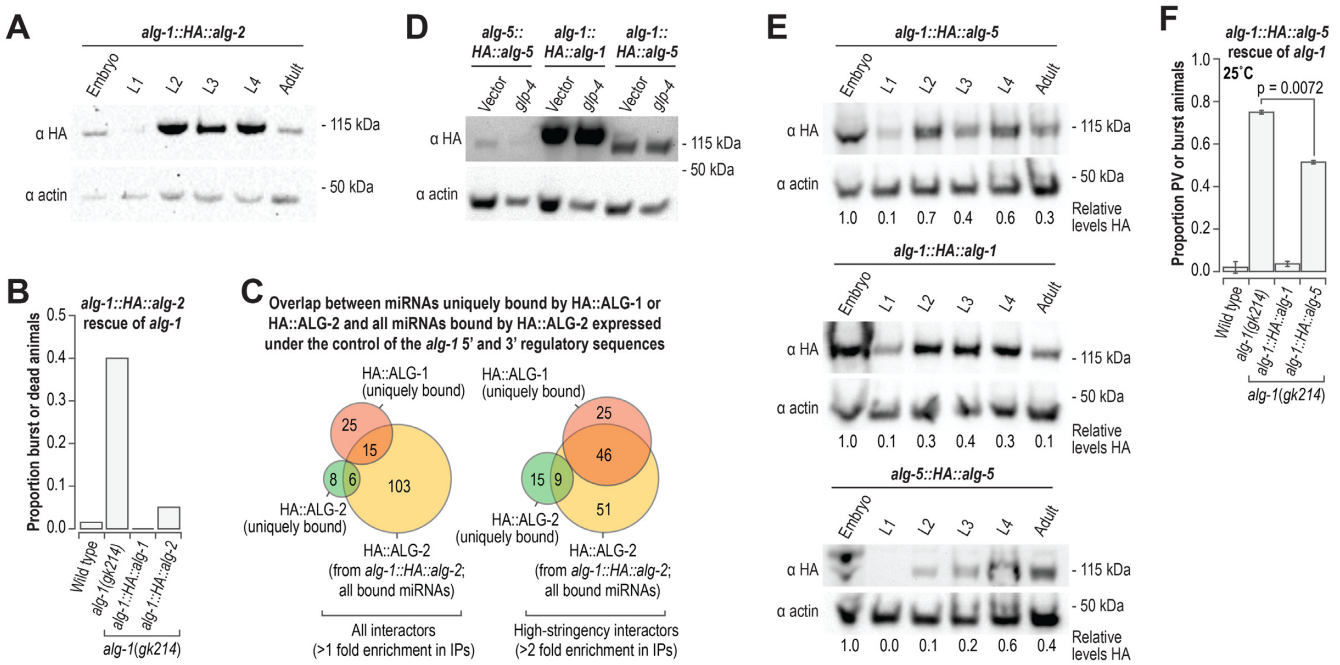


**Figure 7.** Functional overlap of *alg-5, alg-1* and *alg-2*. (**A**) Western blot assay of HA::ALG-2 derived from a chimeric construct containing *alg-1* 5′ and 3′ regulatory sequence and *alg-2* coding sequence (*alg-1::HA::alg-2*). Actin is shown as a loading control. (**B**) Proportion of burst or dead animals. Wild type ($n = 152$), *alg-1(gk214)* ($n = 114$), *alg-1::HA::alg-1; alg-1(gk214)* ($n = 116$), and *alg-1::HA::alg-2; alg-1(gk214)* ($n = 92$) animals were grown at 20°C. (**C**) Overlap of miRNAs enriched >1-fold (left) and >2-fold (right) in co-IP of HA::ALG-2 derived from *alg-1::HA::alg-2; alg-1(gk214)* with miRNAs uniquely enriched in co-IPs from HA::ALG-1 (*alg-1::HA::alg-1; alg-1(gk214)*) or HA::ALG-2 (*alg-2::HA::alg-2; alg-2(ok304)*) co-IPs >1-fold (left) and >2-fold (right). (**D**) Western blot assay of HA::ALG-5 derived from a construct containing the authentic *alg-5* regulatory elements in the *alg-5(tm1163)* mutant background (*alg-5(tm1163); alg-5::HA::alg-5*) and a chimeric construct containing *alg-1* 5′ and 3′ regulatory sequences and *alg-5* coding sequence in the *alg-1(gk214)* mutant background (*alg-1::HA::alg-5; alg-1(gk214)*). HA::ALG-1 from *alg-1::HA::alg-1* in the *alg-1(gk214)* mutant background is also shown. Actin is shown as a loading control. *glp-4* RNAi was done to reduce germ cell proliferation during development. L4440 vector RNAi was done as a control. (**E**) A developmental time course of HA::ALG-5 from *alg-1::HA::alg-5; alg-1(gk214)* (upper panel) and *alg-5(tm1163); alg-5::HA::alg-5* (lower panel) and HA::ALG-1 from *alg-1::HA::alg-1; alg-1(gk214)* (middle panel). Actin is shown as a loading control. Numbers below blot images are signal intensities of HA normalized to actin (embryo samples arbitrarily set to 1.0). (**F**) Proportions of animals containing protruding or burst vulvas. Error bars represent standard deviations from the means from two independent experiments. Wild type ($n = 104$–124), *alg-1(gk214)* ($n = 102$–109), *alg-1::HA::alg-1; alg-1(gk214)* ($n = 109$–114) and *alg-1::HA::alg-5; alg-1(gk214)* ($n = 102$–116) animals were grown at 25°C See also Supplementary Figure S6.

*gans* (16). We then crossed the *alg-1::HA::alg-5* transgene into *alg-1(gk214)* mutants. Given that *alg-5* is normally expressed primarily in the germline and *alg-1* is expressed in the soma (Figure 2E), we tested whether *alg-5* would display somatic expression similar to *alg-1* when expressed from *alg-1* regulatory elements. To suppress germline development, we treated *alg-1::HA::alg-5*-transgenic animals with *glp-4* RNAi. As controls, we included *alg-1::HA::alg-1* and *alg-5::HA::alg-5* transgenic animals. ALG-5 levels in *alg-5(tm1163); alg-5::HA::alg-5* were moderately depleted upon treatment with *glp-4* RNAi compared to treatment with a vector control (Figure 7D). In contrast, the levels of ALG-5 produced from *alg-1::HA::alg-5; alg-1(gk214)* and ALG-1 from *alg-1::HA::alg-1; alg-1(gk214)* were unchanged between vector control RNAi and *glp-4* RNAi (Figure 7D). HA::ALG-5 protein was produced at higher levels when expressed from *alg-1::HA::alg-5* than when expressed from the authentic *alg-5* regulatory elements (*alg-5::HA::alg-5*), but did not appear to be produced at as high of levels as the HA::ALG-1 protein produced from *alg-1::HA::alg-1* (Figure 7D). Thus, it is likely that there are additional features that affect *alg-5* expression or the stability of the ALG-5 protein. The pattern of HA::ALG-5 expression from the *alg-1::HA::alg-5* transgene across development was similar to that of HA::ALG-1 expressed from *alg-1::HA::alg-1* (Figure 7E).

Keeping in mind the caveat that *alg-1::HA::alg-5* does not produce as much protein as *alg-1::HA::alg-1*, we assessed whether *alg-1::HA::alg-5* would rescue the developmental defects in *alg-1(gk214)* mutants. A modest reduction in the proportion of animals displaying protruding or bursting vulvas was observed in *alg-1::HA::alg-5; alg-1(gk214)* animals relative to non-transgenic *alg-1(gk214)* animals when grown at 25°C ($P = 0.0072$, Figure 7F). Thus, ALG-5 likely has some functional overlap with ALG-1 but differences in expression levels prevent us from drawing conclusions about the extent of such overlap.

## DISCUSSION

### ALG-5 as a distinct branch of the miRNA pathway

ALG-5 likely defines a branch of the miRNA pathway largely distinct from that of ALG-1 and ALG-2. ALG-1 and ALG-2 bind overlapping and extensive sets of miRNAs and function redundantly during embryogenesis and larval development (39,44,48). In contrast, ALG-5 binds a

very narrow subset of miRNAs and does not appear to have substantial functional overlap with ALG-1 or ALG-2 despite the three Argonautes having many miRNA interactors in common. Unlike ALG-1 and ALG-2, with central roles in embryogenesis and larval development, ALG-5 appears to have a specific role in developmental timing in the germline. *alg-5* is expressed primarily, if not exclusively, in the germline. *alg-5* mutants display a slight reduction in the number of progeny they produce and an accelerated transition from spermatogenesis to oogenesis. We identified several genes misregulated in *alg-5(ram2)* mutants that could contribute to the observed phenotype, including genes regulating the MAPK pathway, DNA-damage response, and apoptosis. Numerous genes involved in immunity and defense also emerged as being downregulated in *alg-5* mutants. Interestingly, *alg-5* was identified in a screen for gene inactivations that cause hypersensitivity to bacterial pore-forming toxins, hence its original name *hypersensitive to pore-forming toxin-24* (*hpo-24*) (56). Consistent with this role, two genes required for pore-forming toxin defense, the activator protein-1 (AP-1) transcription factors *jun-1* and *fos-1* (56) were downregulated in *alg-5* mutants. It will be important in future studies to identify the direct targets of ALG-5 and its precise function in germline development and pathogen defense.

### ALG-5 localization to P granules

Several Argonautes have been shown to associate with perinuclear germ granules called P granules in *C. elegans*, including the piRNA-associated Argonaute PRG-1 and two siRNA-associated Argonautes, CSR-1 and WAGO-1, where they have important roles in both gene licensing and silencing (13,24,57). Our results demonstrate that ALG-5 also associates with P granules, indicating that miRNAs have a role in regulating gene expression in P granules as well. Interestingly, AIN-1, a GW182 protein orthologous to human TNRC6A, co-purifies with several P granule components (58). GW182 proteins function as scaffolds between miRNA-associated Argonautes and downstream effectors of miRNA-mediated silencing (8). Based on sequence alignment of ALG-5 with human AGO2 and ALG-1, the amino acid residues in the tryptophan binding pockets that facilitate GW182–Argonaute interactions appear to be conserved (Supplementary Figure S1B) (59,60). Thus, AIN-1 may interact with ALG-5 within P granules to mediate RNA silencing.

### Functional similarity between the miRNA-associated Argonautes

ALG-1 but not ALG-2 is required for normal development, despite that the two genes are nearly identical in amino acid sequence (88% identity). ALG-2 expressed under the control of the *alg-1* regulatory sequences largely rescues developmental defects in *alg-1* mutants, indicating that differences in gene expression and not molecular functionality likely distinguish ALG-1 and ALG-2. ALG-5 shares only ∼36% identity with ALG-1 and ALG-2 and is thus unlikely to have identical molecular functionality. ALG-5 lacks the conserved RNaseH residues that confer slicer activity and which are present in ALG-1 and ALG-2, pointing to at least one functional difference between the proteins (10). Nonetheless, when introduced into an *alg-1* mutant under the control of *alg-1* non-coding regulatory sequences, we did observe partial rescue of the *alg-1* mutant phenotype by *alg-5*. The ALG-5 branch of the AGO subfamily is highly conserved across *Caenorhabditis* species estimated to be separated from *C. elegans* by at least 110 million generations (61,62), pointing to ancient divergence of ALG-5 from ALG-1 and ALG-2.

### A near-comprehensive miRNA–Argonaute interactome

Our datasets provide a near-comprehensive analysis of miRNA–Argonaute interactions in *C. elegans*. The majority (∼80%) of annotated miRNAs, including the strands often annotated as star or passenger, were identified in our analysis of Argonaute–small RNA interactions and were enriched in libraries from at least one Argonaute co-immunoprecipitate (co-IP), although many were present at levels below our stringent 10 normalized reads (reads per million total mapped reads) threshold. Many miRNAs were not enriched in any of the Argonaute co-IPs or were completely absent in all of our datasets. Several of the miRNAs not enriched in any of the Argonaute co-IPs are presumed miRNA stars. However, notably absent guide strand miRNAs include miR-261 and miR-264–miR-273, which were identified computationally (63) but have not been validated using sequencing-based approaches, and miR-4930–miR-4935, many of which are enriched in aged animals (64). The three newly discovered miRNAs represent two new miRNA families and a new member of the miR-58/bantam family. Each of the miRNAs is expressed at relatively low levels, likely explaining why they were not identified or validated in previous analyses. Although it is likely that miRNA identification is approaching saturation in *C. elegans*, new miRNAs continue to be discovered and will likely continue to emerge from analyses of animals grown under non-standard laboratory conditions, such as drug treatment, pathogen exposure and environmental stress.

The various roles of miRNAs and their specific functions in *C. elegans* gene regulation are still poorly understood. The identification of ALG-5 and the near comprehensive analysis of miRNA–Argonaute interactions presented here will provide a valuable framework for discovering new roles for miRNAs in development and disease.

## ACCESSION NUMBERS

All the high-throughput sequencing data described here has been deposited to the Gene Expression Omnibus (GEO) and is available under accession number GSE98935.

## SUPPLEMENTARY DATA

Supplementary Data are available at NAR Online.

## ACKNOWLEDGEMENTS

Thanks to David Fay, Young-Soo (Ellen) Rim and Emily Seward for technical assistance, and John Kim, Tim Schedl and Carolyn Phillips for helpful discussion. Strains were

provided by the Caenorhabditis Genetics Center (CGC), which is funded by the NIH Office of Research Infrastructure Programs (P40 OD010440). High-throughput sequencing was done by Novogene and at the University of Colorado Anschutz Medical Campus Genomics and Microarray Core and the Colorado State University Next Generation Sequencing Facility with assistance from Katrina Diener, Colin Larson, Ted Shade, Erin Petrilli, Mark Stenglein and Justin Lee.

## FUNDING

Colorado State University [laboratory startup funds to T.A.M.]; Boettcher Foundation [003614-00002 to T.A.M.]; NIH [R35 GM119775 to T.A.M.]; Department of Education GAANN fellowship [to K.C.B.]. Funding for open access charge: NIH [R35 GM119775].
*Conflict of interest statement.* None declared.

## REFERENCES

1. Bartel,D.P. (2004) MicroRNAs: genomics, biogenesis, mechanism, and function. *Cell*, **116**, 281–297.
2. Lim,L.P., Lau,N.C., Weinstein,E.G., Abdelhakim,A., Yekta,S., Rhoades,M.W., Burge,C.B. and Bartel,D.P. (2003) The microRNAs of Caenorhabditis elegans. *Genes Dev*, **17**, 991–1008.
3. Lee,Y., Ahn,C., Han,J., Choi,H., Kim,J., Yim,J., Lee,J., Provost,P., Radmark,O., Kim,S. *et al.* (2003) The nuclear RNase III Drosha initiates microRNA processing. *Nature*, **425**, 415–419.
4. Khvorova,A., Reynolds,A. and Jayasena,S.D. (2003) Functional siRNAs and miRNAs exhibit strand bias. *Cell*, **115**, 209–216.
5. Schwarz,D.S., Hutvagner,G., Du,T., Xu,Z., Aronin,N. and Zamore,P.D. (2003) Asymmetry in the assembly of the RNAi enzyme complex. *Cell*, **115**, 199–208.
6. Liu,J., Carmell,M.A., Rivas,F.V., Marsden,C.G., Thomson,J.M., Song,J.J., Hammond,S.M., Joshua-Tor,L. and Hannon,G.J. (2004) Argonaute2 is the catalytic engine of mammalian RNAi. *Science*, **305**, 1437–1441.
7. Bartel,D.P. (2009) MicroRNAs: target recognition and regulatory functions. *Cell*, **136**, 215–233.
8. Jonas,S. and Izaurralde,E. (2015) Towards a molecular understanding of microRNA-mediated gene silencing. *Nat. Rev. Genet.*, **16**, 421–433.
9. Claycomb,J.M. (2014) Ancient endo-siRNA pathways reveal new tricks. *Curr. Biol.*, **24**, R703–R715.
10. Tolia,N.H. and Joshua-Tor,L. (2007) Slicer and the argonautes. *Nat. Chem. Biol.*, **3**, 36–43.
11. Grishok,A. (2013) Biology and mechanisms of short RNAs in Caenorhabditis elegans. *Adv. Genet.*, **83**, 1–69.
12. Correa,R.L., Steiner,F.A., Berezikov,E. and Ketting,R.F. (2010) MicroRNA-directed siRNA biogenesis in Caenorhabditis elegans. *PLoS Genet.*, **6**, e1000903.
13. Gu,W., Shirayama,M., Conte,D. Jr, Vasale,J., Batista,P.J., Claycomb,J.M., Moresco,J.J., Youngman,E.M., Keys,J., Stoltz,M.J. *et al.* (2009) Distinct argonaute-mediated 22G-RNA pathways direct genome surveillance in the C. elegans germline. *Mol. Cell*, **36**, 231–244.
14. Montgomery,T.A., Howell,M.D., Cuperus,J.T., Li,D., Hansen,J.E., Alexander,A.L., Chapman,E.J., Fahlgren,N., Allen,E. and Carrington,J.C. (2008) Specificity of ARGONAUTE7-miR390 interaction and dual functionality in TAS3 trans-acting siRNA formation. *Cell*, **133**, 128–141.
15. Phillips,C.M., Montgomery,T.A., Breen,P.C. and Ruvkun,G. (2012) MUT-16 promotes formation of perinuclear mutator foci required for RNA silencing in the C. elegans germline. *Genes Dev.*, **26**, 1433–1444.
16. Frokjaer-Jensen,C., Davis,M.W., Hopkins,C.E., Newman,B.J., Thummel,J.M., Olesen,S.P., Grunnet,M. and Jorgensen,E.M. (2008) Single-copy insertion of transgenes in Caenorhabditis elegans. *Nat. Genet.*, **40**, 1375–1383.
17. Dickinson,D.J., Ward,J.D., Reiner,D.J. and Goldstein,B. (2013) Engineering the Caenorhabditis elegans genome using Cas9-triggered homologous recombination. *Nat. Methods*, **10**, 1028–1034.
18. Dickinson,D.J., Pani,A.M., Heppert,J.K., Higgins,C.D. and Goldstein,B. (2015) Streamlined genome engineering with a self-excising drug selection cassette. *Genetics*, **200**, 1035–1049.
19. Brenner,S. (1974) The genetics of Caenorhabditis elegans. *Genetics*, **77**, 71–94.
20. Larkin,M.A., Blackshields,G., Brown,N.P., Chenna,R., McGettigan,P.A., McWilliam,H., Valentin,F., Wallace,I.M., Wilm,A., Lopez,R. *et al.* (2007) Clustal W and Clustal X version 2.0. *Bioinformatics*, **23**, 2947–2948.
21. Felsenstein,J. (1989) PHYLIP—Phylogeny Inference Package (Version 3.2). *Cladistics*, **5**, 164–166.
22. Kamath,R.S., Fraser,A.G., Dong,Y., Poulin,G., Durbin,R., Gotta,M., Kanapin,A., Le Bot,N., Moreno,S., Sohrmann,M. *et al.* (2003) Systematic functional analysis of the Caenorhabditis elegans genome using RNAi. *Nature*, **421**, 231–237.
23. Fahlgren,N., Sullivan,C.M., Kasschau,K.D., Chapman,E.J., Cumbie,J.S., Montgomery,T.A., Gilbert,S.D., Dasenko,M., Backman,T.W., Givan,S.A. *et al.* (2009) Computational and analytical framework for small RNA profiling by high-throughput sequencing. *RNA*, **15**, 992–1002.
24. Claycomb,J.M., Batista,P.J., Pang,K.M., Gu,W., Vasale,J.J., van Wolfswinkel,J.C., Chaves,D.A., Shirayama,M., Mitani,S., Ketting,R.F. *et al.* (2009) The Argonaute CSR-1 and its 22G-RNA cofactors are required for holocentric chromosome segregation. *Cell*, **139**, 123–134.
25. Mackowiak,S.D. (2011) Identification of novel and known miRNAs in deep-sequencing data with miRDeep2. *Curr. Protoc. Bioinformatics*, doi:10.1002/0471250953.bi1210s36.
26. Zhang,Z., Theurkauf,W.E., Weng,Z. and Zamore,P.D. (2012) Strand-specific libraries for high throughput RNA sequencing (RNA-Seq) prepared without poly(A) selection. *Silence*, **3**, 9.
27. Bolger,A.M., Lohse,M. and Usadel,B. (2014) Trimmomatic: a flexible trimmer for Illumina sequence data. *Bioinformatics*, **30**, 2114–2120.
28. Kim,D., Pertea,G., Trapnell,C., Pimentel,H., Kelley,R. and Salzberg,S.L. (2013) TopHat2: accurate alignment of transcriptomes in the presence of insertions, deletions and gene fusions. *Genome Biol.*, **14**, R36.
29. Trapnell,C., Roberts,A., Goff,L., Pertea,G., Kim,D., Kelley,D.R., Pimentel,H., Salzberg,S.L., Rinn,J.L. and Pachter,L. (2012) Differential gene and transcript expression analysis of RNA-seq experiments with TopHat and Cufflinks. *Nat. Protoc.*, **7**, 562–578.
30. Anders,S., Pyl,P.T. and Huber,W. (2015) HTSeq—a Python framework to work with high-throughput sequencing data. *Bioinformatics*, **31**, 166–169.
31. Love,M.I., Huber,W. and Anders,S. (2014) Moderated estimation of fold change and dispersion for RNA-seq data with DESeq2. *Genome Biol.*, **15**, 550.
32. Huang da,W., Sherman,B.T. and Lempicki,R.A. (2009) Systematic and integrative analysis of large gene lists using DAVID bioinformatics resources. *Nat. Protoc.*, **4**, 44–57.
33. Huang da,W., Sherman,B.T. and Lempicki,R.A. (2009) Bioinformatics enrichment tools: paths toward the comprehensive functional analysis of large gene lists. *Nucleic Acids Res.*, **37**, 1–13.
34. Hulsen,T., de Vlieg,J. and Alkema,W. (2008) BioVenn - a web application for the comparison and visualization of biological lists using area-proportional Venn diagrams. *BMC Genomics*, **9**, 488.
35. Robinson,J.T., Thorvaldsdottir,H., Winckler,W., Guttman,M., Lander,E.S., Getz,G. and Mesirov,J.P. (2011) Integrative genomics viewer. *Nat. Biotechnol.*, **29**, 24–26.
36. Thorvaldsdottir,H., Robinson,J.T. and Mesirov,J.P. (2013) Integrative Genomics Viewer (IGV): high-performance genomics data visualization and exploration. *Brief. Bioinform.*, **14**, 178–192.
37. Jan,C.H., Friedman,R.C., Ruby,J.G. and Bartel,D.P. (2011) Formation, regulation and evolution of Caenorhabditis elegans 3′UTRs. *Nature*, **469**, 97–101.
38. Lewis,B.P., Burge,C.B. and Bartel,D.P. (2005) Conserved seed pairing, often flanked by adenosines, indicates that thousands of human genes are microRNA targets. *Cell*, **120**, 15–20.
39. Grishok,A., Pasquinelli,A.E., Conte,D., Li,N., Parrish,S., Ha,I., Baillie,D.L., Fire,A., Ruvkun,G. and Mello,C.C. (2001) Genes and mechanisms related to RNA interference regulate expression of the

small temporal RNAs that control C. elegans developmental timing. *Cell*, **106**, 23–34.
40. Bukhari,S.I., Vasquez-Rifo,A., Gagne,D., Paquet,E.R., Zetka,M., Robert,C., Masson,J.Y. and Simard,M.J. (2012) The microRNA pathway controls germ cell proliferation and differentiation in C. elegans. *Cell Res.*, **22**, 1034–1045.
41. Yuan,Y.R., Pei,Y., Ma,J.B., Kuryavyi,V., Zhadina,M., Meister,G., Chen,H.Y., Dauter,Z., Tuschl,T. and Patel,D.J. (2005) Crystal structure of A. aeolicus argonaute, a site-specific DNA-guided endoribonuclease, provides insights into RISC-mediated mRNA cleavage. *Mol. Cell*, **19**, 405–419.
42. Cutter,A.D. (2004) Sperm-limited fecundity in nematodes: how many sperm are enough? *Evolution*, **58**, 651–655.
43. Hodgkin,J. and Barnes,T.M. (1991) More is not better: brood size and population growth in a self-fertilizing nematode. *Proc. Biol. Sci.*, **246**, 19–24.
44. Vasquez-Rifo,A., Jannot,G., Armisen,J., Labouesse,M., Bukhari,S.I., Rondeau,E.L., Miska,E.A. and Simard,M.J. (2012) Developmental characterization of the microRNA-specific C. elegans Argonautes alg-1 and alg-2. *PLoS One*, **7**, e33750.
45. Zinovyeva,A.Y., Bouasker,S., Simard,M.J., Hammell,C.M. and Ambros,V. (2014) Mutations in conserved residues of the C. elegans microRNA Argonaute ALG-1 identify separable functions in ALG-1 miRISC loading and target repression. *PLoS Genet.*, **10**, e1004286.
46. Zinovyeva,A.Y., Veksler-Lublinsky,I., Vashisht,A.A., Wohlschlegel,J.A. and Ambros,V.R. (2015) Caenorhabditis elegans ALG-1 antimorphic mutations uncover functions for Argonaute in microRNA guide strand selection and passenger strand disposal. *Proc. Natl. Acad. Sci. U.S.A.*, **112**, E5271–5280.
47. Tops,B.B., Plasterk,R.H. and Ketting,R.F. (2006) The Caenorhabditis elegans Argonautes ALG-1 and ALG-2: almost identical yet different. *Cold Spring Harb. Symp. Quant. Biol.*, **71**, 189–194.
48. Bouasker,S. and Simard,M.J. (2012) The slicing activity of miRNA-specific Argonautes is essential for the miRNA pathway in C. elegans. *Nucleic Acids Res.*, **40**, 10452–10462.
49. Billi,A.C., Fischer,S.E.J. and Kim,J.K. (2014) Endogenous RNAi pathways in C. elegans. *WormBook*, 1–49.
50. Alvarez-Saavedra,E. and Horvitz,H.R. (2010) Many families of C. elegans microRNAs are not essential for development or viability. *Curr. Biol.*, **20**, 367–373.
51. Kato,M., Chen,X., Inukai,S., Zhao,H. and Slack,F.J. (2011) Age-associated changes in expression of small, noncoding RNAs, including microRNAs, in C. elegans. *RNA*, **17**, 1804–1820.
52. Massirer,K.B., Perez,S.G., Mondol,V. and Pasquinelli,A.E. (2012) The miR-35-41 family of microRNAs regulates RNAi sensitivity in Caenorhabditis elegans. *PLoS Genet.*, **8**, e1002536.
53. Conine,C.C., Batista,P.J., Gu,W., Claycomb,J.M., Chaves,D.A., Shirayama,M. and Mello,C.C. (2010) Argonautes ALG-3 and ALG-4 are required for spermatogenesis-specific 26G-RNAs and thermotolerant sperm in Caenorhabditis elegans. *Proc. Natl. Acad. Sci. U.S.A.*, **107**, 3588–3593.
54. Conine,C.C., Moresco,J.J., Gu,W., Shirayama,M., Conte,D. Jr, Yates,J.R. 3rd and Mello,C.C. (2013) Argonautes promote male fertility and provide a paternal memory of germline gene expression in C. elegans. *Cell*, **155**, 1532–1544.
55. Han,T., Manoharan,A.P., Harkins,T.T., Bouffard,P., Fitzpatrick,C., Chu,D.S., Thierry-Mieg,D., Thierry-Mieg,J. and Kim,J.K. (2009) 26G endo-siRNAs regulate spermatogenic and zygotic gene expression in Caenorhabditis elegans. *Proc. Natl. Acad. Sci. U.S.A.*, **106**, 18674–18679.
56. Kao,C.Y., Los,F.C., Huffman,D.L., Wachi,S., Kloft,N., Husmann,M., Karabrahimi,V., Schwartz,J.L., Bellier,A., Ha,C. *et al.* (2011) Global functional analyses of cellular responses to pore-forming toxins. *PLoS Pathog.*, **7**, e1001314.
57. Batista,P.J., Ruby,J.G., Claycomb,J.M., Chiang,R., Fahlgren,N., Kasschau,K.D., Chaves,D.A., Gu,W., Vasale,J.J., Duan,S. *et al.* (2008) PRG-1 and 21U-RNAs interact to form the piRNA complex required for fertility in C. elegans. *Mol. Cell*, **31**, 67–78.
58. Wu,E., Vashisht,A.A., Chapat,C., Flamand,M.N., Cohen,E., Sarov,M., Tabach,Y., Sonenberg,N., Wohlschlegel,J. and Duchaine,T.F. (2017) A continuum of mRNP complexes in embryonic microRNA-mediated silencing. *Nucleic Acids Res.*, **45**, 2081–2098.
59. Schirle,N.T. and MacRae,I.J. (2012) The crystal structure of human Argonaute2. *Science*, **336**, 1037–1040.
60. Jannot,G., Michaud,P., Quevillon Huberdeau,M., Morel-Berryman,L., Brackbill,J.A., Piquet,S., McJunkin,K., Nakanishi,K. and Simard,M.J. (2016) GW182-free microRNA silencing complex controls post-transcriptional gene expression during Caenorhabditis elegans embryogenesis. *PLoS Genet.*, **12**, e1006484.
61. Shi,Z., Montgomery,T.A., Qi,Y. and Ruvkun,G. (2013) High-throughput sequencing reveals extraordinary fluidity of miRNA, piRNA, and siRNA pathways in nematodes. *Genome Res.*, **23**, 497–508.
62. Cutter,A.D., Dey,A. and Murray,R.L. (2009) Evolution of the Caenorhabditis elegans genome. *Mol. Biol. Evol.*, **26**, 1199–1234.
63. Grad,Y., Aach,J., Hayes,G.D., Reinhart,B.J., Church,G.M., Ruvkun,G. and Kim,J. (2003) Computational and experimental identification of C. elegans microRNAs. *Mol. Cell*, **11**, 1253–1263.
64. de Lencastre,A., Pincus,Z., Zhou,K., Kato,M., Lee,S.S. and Slack,F.J. (2010) MicroRNAs both promote and antagonize longevity in C. elegans. *Curr. Biol.*, **20**, 2159–2168.